Letter

High-temperature superconductivity in La_4H_{23} below 100 GPa

Sam Cross [1,*] Jonathan Buhot [1] Annabelle Brooks [1,2] William Thomas [1] Annette Kleppe [2] Oliver Lord [3] and Sven Friedemann [1,†]

[1]*HH Wills Laboratory, University of Bristol, Bristol BS8 1TL, United Kingdom*
[2]*Diamond Light Source, Chilton, Oxfordshire OX11 0DE, United Kingdom*
[3]*Department of Earth Sciences, University of Bristol, Bristol BS8 1RJ, United Kingdom*

(Received 17 August 2023; revised 29 November 2023; accepted 8 December 2023; published 12 January 2024)

High-temperature superconductivity has been observed in binary hydrides such as LaH_{10} at pressures close to 180 GPa, whereby hydrogen cagelike structures have been identified as a common motif beneficial for high critical temperatures T_c. Efforts are now focused on finding hydride high-temperature superconductors at lower pressures. We present evidence for high-temperature superconductivity in binary La_4H_{23} at a pressure of $P = 95$ GPa, with A15-type arrangement of the lanthanum atoms in the type-I clathrate structure. We synthesize La_4H_{23} from a lanthanum film capped with a palladium catalyst promoting the dissociation of hydrogen. In resistance measurements, we observe superconductivity with a transition temperature $T_c \sim 90$ K. The A15-type lanthanum sublattice is identified in x-ray diffraction on the same sample, in agreement with previous x-ray diffraction and structure prediction studies. Our study reinforces the favorability of cagelike networks of the hydrogen lattice for high-temperature superconductivity.

DOI: 10.1103/PhysRevB.109.L020503

Introduction. High-temperature superconductivity up to 250 K has been reported and independently confirmed in cubic $Fm\bar{3}m$ LaH_{10} at pressures of around 180 GPa [1,2]. In LaH_{10} and other hydride high-temperature superconductors, clathratelike cages of hydrogen atoms surrounding each metal atom have been identified as a common structural motif [3,4]. Recent efforts have been devoted to finding high-temperature superconducting phases at lower pressures [4]. Notably, the high-T_c phase discovered in the La-Ce-H ternary system could be stabilized at moderate pressures around 100 GPa [5]. A recent x-ray diffraction (XRD) study has identified the type-I clathrate structure in binary lanthanum hydride (space group $Pm\bar{3}n$) with the empirical formula La_4H_{23} [6]. The structure features clathratelike hydrogen cages and hence is a strong candidate for superconductivity.

The type-I clathrate structure of La_4H_{23} comprises cagelike networks of hydrogen atoms around a cubic arrangement of the lanthanum atoms, as illustrated in Fig. 1(d). In this structure, the lanthanum atoms occupy the 6*c* and 2*a* Wyckoff sites in an A15-type arrangement, while the hydrogen atoms are predicted to adopt a Weaire-Phelan structure comprising two distinct hydrogen cagelike structures [7], namely, H_{20} dodecahedra and H_{24} tetrakaidecahedra, as shown by the green and orange cages, respectively, in Fig. 1(d). The hydrogen atoms feature bond lengths in the range ≈ 1.1 to 1.3 Å that is favorable for high-temperature superconductivity [8]. This bond length is much larger than in hydrogen molecules at this pressure and indicates a weaker bond compared to molecular bonding [7]. Through the donation of electrons from the metal atoms, the hydrogen antibonding bands can be populated, leading to stabilization of the hydrogen cages and providing an avenue for metallization and superconductivity [9]. The weakening of the H-H bond and the formation of cages is required for hydrogen to contribute electronic states at the Fermi energy and hence for significant electron-phonon coupling involving the hydrogen atoms required for high-temperature superconductivity.

Hydride compounds adopting the type-I clathrate structure have been investigated for superconductivity in computational studies, e.g., leading to the prediction of high-temperature superconductivity in $LiNa_3H_{23}$ [10]. Recently, superconductivity was indeed discovered in members of this structure type, in Lu_4H_{23} at pressures above 200 GPa [11]. Furthermore, the structure type has also been detected in x-ray diffraction studies of Ba_4H_{23}, Eu_4H_{23}, La_4H_{23}, and Y_4H_{23} [6,7,12,13]. Hence, there is a strong interest to probe experimentally for superconductivity in members of this structure type.

The A15-type sublattice of La_4H_{23} has recently been detected with single-crystal XRD by Laniel *et al.* at pressures from 96 GPa to 150 GPa [6]. Laniel *et al.* synthesized La_4H_{23} by laser heating bulk lanthanum with paraffin oil as a hydrogen donor material. Recently, Guo *et al.* reported synthesis of La_4H_{23} from bulk LaH_3 and ammonia borane (AB, NH_3BH_3) [14]. Furthermore, Guo *et al.* detected superconductivity in their samples of La_4H_{23} in resistance measurements. Here, we present the synthesis of La_4H_{23} at 95 GPa from a thin film of lanthanum capped with palladium

*sc16434@bristol.ac.uk
†sven.friedemann@bristol.ac.uk

Published by the American Physical Society under the terms of the Creative Commons Attribution 4.0 International license. Further distribution of this work must maintain attribution to the author(s) and the published article's title, journal citation, and DOI.

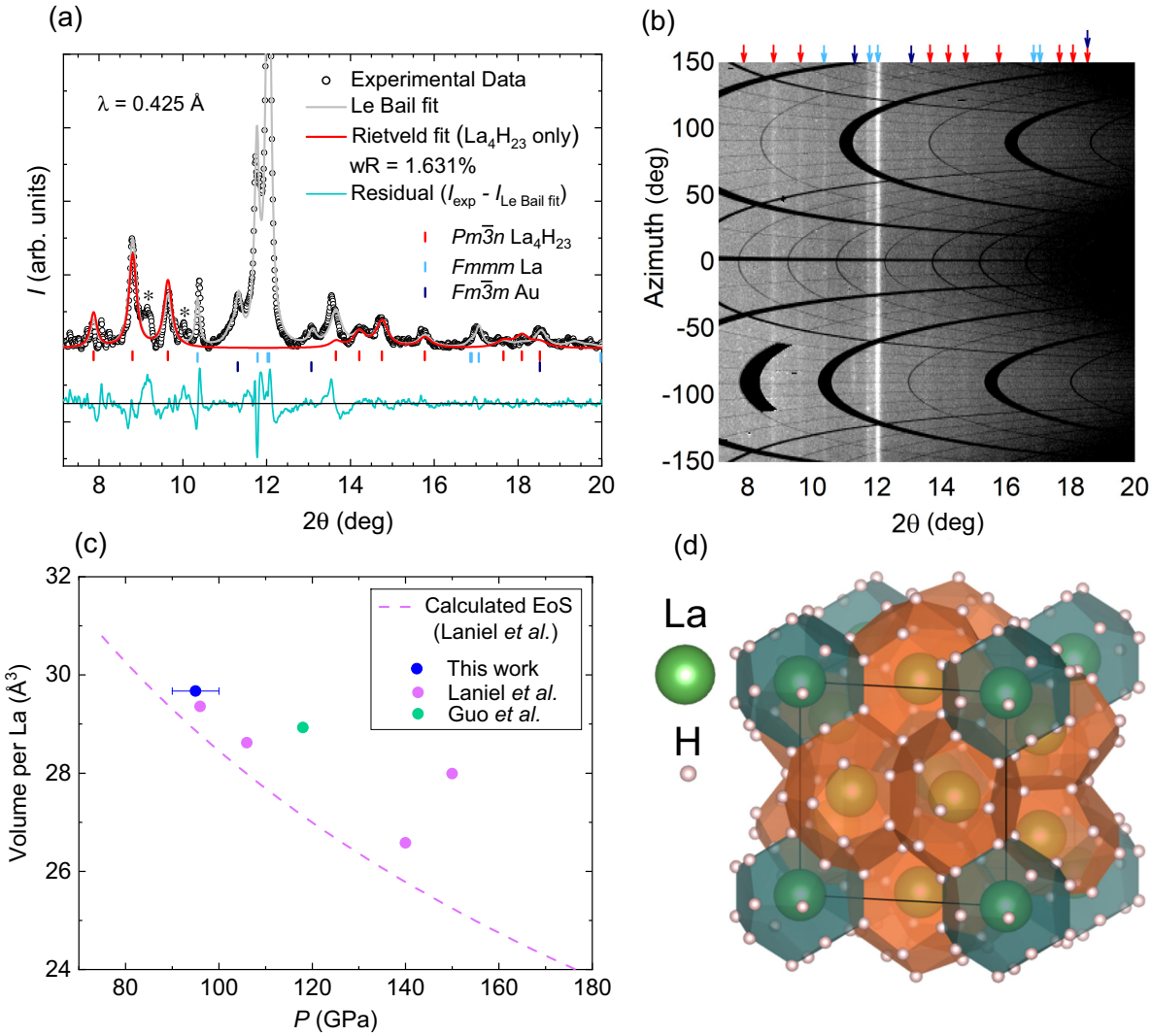

FIG. 1. Detection of La_4H_{23} in x-ray diffraction at 95 GPa. (a) Rietveld and Le Bail refinements of La_4H_{23} to the observed XRD pattern shown by the solid red and gray lines, respectively. Data between 11° to 13° are dominated by residual elemental lanthanum in the orthorhombic $Fmmm$ phase and gold in the cubic $Fm\bar{3}m$ phase originating from the electrodes. No La_4H_{23} reflections are expected in this range. Unassigned reflections at 9° and 10° are marked with an asterisk (∗). (b) Azimuthal (cake) plot representation of the area detector image in grayscale with background correction to enhance contrast (details in *methods*). High and low intensity are represented in white and black, respectively. Sample reflections appear as white vertical lines, with each phase indicated by the arrows with the same color code as in (a). (c) Unit-cell volume as a function of pressure for the La_4H_{23} phase including data from this work, and that of Refs. [6,14]. (d) Picture of the ideal type-I clathrate structure of La_4H_{23} generated using VESTA [18].

and using NH_3BH_3 as a hydrogen donor. The palladium capping layer prevents oxidation of the lanthanum film and acts to facilitate hydrogenation of the film on laser heating [15]. We detect the formation of La_4H_{23} with XRD measurements and superconductivity through four-point resistance measurements including the characteristic suppression in magnetic fields up to 12 T.

Synthesis of La_4H_{23}. The successful synthesis of La_4H_{23} is evident from our x-ray diffraction in Fig. 1. We observe characteristic reflections in the range $7.5° \leqslant 2\theta \leqslant 10°$ and $13.5° \leqslant 2\theta \leqslant 16°$ that are best assigned to the La_4H_{23} phase. Besides the La_4H_{23}, we also observe peaks from elemental lanthanum ($Fmmm$) and gold ($Fm\bar{3}m$). The former is residue from the synthesis of La_4H_{23}, while the latter originates from the electrodes used for our resistance measurements. We can rule out several other phases including $I4/mmm$ LaH_4, $P6_3/mmc$ LaH_9, and $C2/m$ LaH_x that have been reported for the La-H binary system (see Figs. S1–S3 of the Supplemental Material [16]). We can also rule out the formation of $Fm\bar{3}m$ $LaBH_8$ [17] as well as the carbohydride impurity $P6_3/mmc$ $LaCH_2$ reported by Laniel *et al.* at 96 GPa [6] (see Figs. S4 and S5 of the Supplemental Material [16]).

The XRD data reveal a homogeneous La_4H_{23} sample without preferred orientation of its crystallites. This is visible from both the azimuthal representation of the detector image in Fig. 1(b) and the analysis of the angle-integrated XRD pattern. The detector image shows continuous vertical lines associated with La_4H_{23} [red arrows in Fig. 1(b)] without significant spots indicating a large ensemble of grains in a polycrystalline sample. At the same time, the angle-integrated XRD pattern

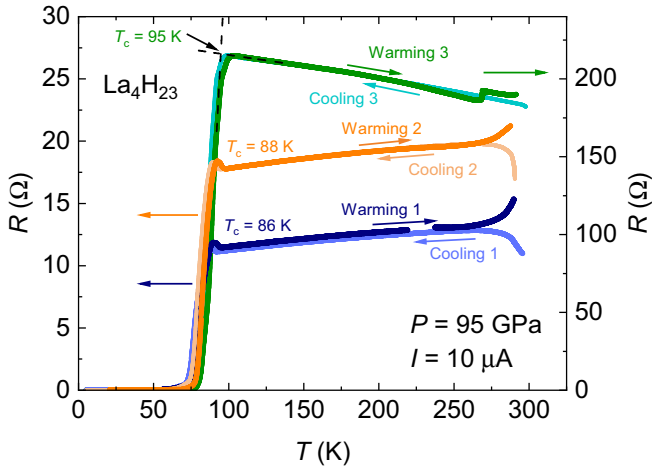

FIG. 2. Detection of superconductivity in La_4H_{23} and resistance measurements on subsequent cooling runs. In each case, cooling and warming measurements are indicated. The value of T_c was determined at the onset of superconductivity from the intersection of linear fits to the normal and superconducting states, shown by the dashed line in the third thermal cycle. Cool-down and warm-up 1 and 2 were collected shortly after laser heating. Cool-down and warm-up 3 were recorded after the XRD measurements. The absence of data between 220 K and 235 K in warming cycle 1 was due to a glitch in the data acquisition. The step change in the resistance observed at ∼260 K in warming cycle 3 was due to an unintentional pause for several hours.

exhibits peak intensities as expected for a powder average [Fig. 1(a)]. Indeed, we are able to fit the observed XRD pattern with a Rietveld refinement of La_4H_{23} without any preferential orientation, only invoking strain to reproduce the peak broadening.

The lattice constants extracted from Rietveld refinement provide confidence in the assignment of the La_4H_{23} phase with an A15-type La sublattice and suggest a large hydrogen content close to the stoichiometric ratio La:H = 1:5.75 for the La_4H_{23} phase. The lattice parameters [$a = 6.191(4)$ Å, volume per La atom = 29.66(8) Å^3] are in good agreement with previous reports and close to the predicted equation of state (EoS), as shown in Fig. 1(c) [6]. The comparison with the EoS suggests a stoichiometric La_4H_{23} composition. However, some uncertainty remains for this indirect method of determining the hydrogen content, as pointed out by Laniel *et al.* [6]. In particular, we cannot exclude vacancies on the hydrogen lattice and have limited resolution to detect the subtle modifications of the metal sublattice that might be associated with hydrogen vacancies [7].

High-temperature superconductivity in La_4H_{23}. The resistance measurements presented in Fig. 2 provide evidence for high-temperature superconductivity in La_4H_{23}. Immediately after laser heating, we observe a pronounced drop in the resistance with an onset at $T_c = 86$ K and reaching zero resistance within the resolution $|R - R_n|/R_n \leqslant 1 \times 10^{-3}$ of our experiment below 60 K, where R_n is the resistance of the normal state. The measured value of T_c is in very good agreement with that of Guo *et al.*, where palladium was not used as part of the synthesis [14], thus ruling out superconductivity originating from a thin PdH_x layer and providing confidence in our assignment of T_c to the La_4H_{23} phase. We have repeated resistance measurements several times, including before and after XRD measurements, and find the superconductivity to be stable with a slight increase to $T_c = 95$ K between subsequent measurements. We attribute this increase to annealing of the sample at room temperature, similar to reports on H_3S [19].

The normal state resistance shows indications of phase instabilities, which we assign to decomposition exhibiting activated behavior. If warming the sample above 250 K, the sample resistance increases as a function of time, as illustrated in Fig. 2. This manifests as an initial increase during cool-downs and further increase during warm-up. Only below 250 K do cool-down and warm-up agree, where we observe metallic behavior in the sample immediately after laser heating (thermal cycles 1 and 2).

The changes to the sample also induce a fundamental change from metallic to nonmetallic over time. Over multiple warm-ups to above 250 K, the resistance changes from metallic ($dR/dT > 0$) to nonmetallic ($dR/dT < 0$). A similar change from metallic to nonmetallic has been observed by Guo *et al.* after laser heating and in subsequent decompression runs. In our study, the pressure before and after laser heating remained the same within our uncertainty of ±5 GPa. Therefore the change in the normal state could originate from either smaller changes in pressure (< 5 GPa) and/or could be time dependent. Equally, the broadening of the superconducting transition and the loss of zero resistance reported by Guo *et al.* upon decompression to below 100 GPa may be related to sample decomposition.

The combination of increasing resistance and change to nonmetallic behavior suggests that part of the sample slowly transforms to a semimetallic or insulating material. In our sample, we have detected La_4H_{23} and elemental La with XRD, both of which may form part of the electrical path sampled by our resistance measurements with La_4H_{23} providing at least a percolative path supporting zero resistance of the high-T_c state. Hence, the increase in resistance with time above 250 K could be a conversion of either La_4H_{23} or La to a semimetallic or insulating phase, e.g., LaH_3, which has been reported to become semimetallic at high pressures [2]. We argue that La_4H_{23} is converting because Guo *et al.* observe a very similar change from metallic to nonmetallic, but do not have elemental lanthanum in their pressure cell. We note that LaH_3 has been ruled out as a high-T_c material [2] and could remain undetected in XRD in the presence of La_4H_{23} (see Fig. S6 of the Supplemental Material [16]). In our sample, the volume fraction of La_4H_{23}, while decreasing, retains a full path to detect zero resistance during the course of our measurements, while in the study of Guo *et al.*, the nonzero resistance below 100 GPa suggests that a larger portion of the sample has transformed to a semimetallic state.

The change in resistance may be related to the thermodynamic instability found in density functional theory (DFT) calculations by Guo *et al.* [14]. At 100 GPa, the DFT predicts that La_4H_{23} is above the convex hull by a small energy, which could lead to disintegration with an activation energy. In addition, the presence of imaginary phonons suggests dynamical instability of the phase in the harmonic limit. The observed presence of La_4H_{23} in the studies by Laniel, Guo, and in the

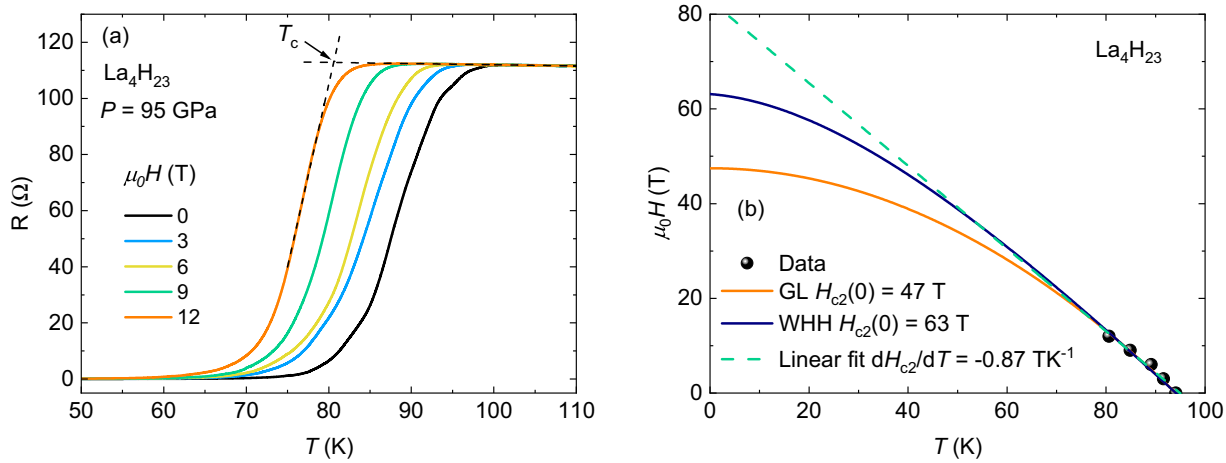

FIG. 3. Superconducting critical field of La_4H_{23}. (a) Temperature sweeps for different magnetic fields. The value of T_c was determined at the onset of superconductivity, as shown by the dashed line for the 12 T curve. (b) Temperature dependence of the upper critical field with Ginzburg-Landau (GL) and Werthamer-Helfand-Hohenberg (WHH) fits to estimate $H_{c2}(0)$, and a linear fit to extract the gradient near T_c.

present work demonstrate that likely anharmonic corrections arising due to quantum fluctuations of the hydrogen lattice are necessary to stabilize the structure. Indeed, both high-T_c hydrides LaH_{10} and H_3S are stabilized by quantum effects [20,21]. Further investigations are required to map the stability range of the La_4H_{23} phase, including under the influence of excess or deficiency of hydrogen in the diamond anvil cell (DAC). So far, all reported syntheses have employed hydrogen donor materials such as NH_3BH_3 and paraffin. It will be of interest to check if a synthesis in excess molecular hydrogen shows a larger stability range to lower pressures. Further x-ray diffraction studies to probe the decomposition are equally desirable.

The suppression of the resistive transition in a magnetic field provides further evidence for superconductivity in La_4H_{23}. The transition is suppressed by 13 K in a magnetic field of 12 T as illustrated in Fig. 3(a).

We extract $T_c(H)$ in order to map the temperature dependence of the upper critical field $H_{c2}(T)$, as shown in Fig. 3(b), where the zero-temperature value $H_{c2}(0)$ is estimated from extrapolations of the Ginzburg-Landau (GL) and the simplified Werthamer-Helfand-Hohenberg (WHH) models [22], yielding 47 T and 63 T, respectively. The linear regime of the critical field, $H_{c2}(T)$, can be used to estimate the zero-temperature coherence length ξ_0 of the superconducting state and the Fermi velocity v_F of the normal state. Using the clean-limit expression and the slope of the critical field near T_c ($dH_{c2}/dT = -0.87$ TK^{-1}), we obtain $\xi_0 = 2.7$ nm. The change of the resistance to nonmetallic indicates that the sample requires a dirty-limit expression. In the absence of direct or indirect measurements that allow one to estimate the mean free path, the dirty-limit expressions cannot be used to extract ξ_0. However, the clean-limit expression still provides a good estimate and likely only small corrections will arise from the dirty-limit behavior. Indeed, the comparable slope of $H_{c2}(T)$ observed by Guo *et al.* suggests that both studies observe the intrinsic behavior of La_4H_{23}.

The Fermi velocity is estimated as $v_F = 1.8 \times 10^5$ ms^{-1}. This value is lower compared to H_3S [23]. Likely, this reflects a reduced renormalization and hence a weaker electron-phonon coupling compared to H_3S, in agreement with the lower T_c. A more accurate estimation of the renormalization requires detailed band structure calculations based on a stable structure.

Conclusion. The discovery of high-temperature superconductivity in La_4H_{23} with an A15-type arrangement of the lanthanum atoms in the type-I clathrate structure reinforces that cagelike networks of the hydrogen lattice are beneficial for high-T_c superconductivity. This structure type is, so far, the prime example of how high-temperature superconductivity can be realized below 100 GPa in a binary hydride material. The XRD analysis suggests that La_4H_{23} is the major phase synthesized at pressures around 100 GPa. This may help forming pure samples in the future to study the intrinsic superconducting properties and hence has the potential to advance the understanding of high-temperature superconductivity in hydride compounds.

Methods. High pressures were achieved in a DAC machined from MP35N alloy, with diamond anvils of culet diameter 50 μm bevelled at 8° to a diameter of 300 μm. Gaskets were prepared by pre-indentation of 250 μm steel 301 and insulated with a boron nitride and epoxy mixture. The insulation was indented to a thickness 30 μm and a sample space of diameter 28 μm was drilled. The anvil with the sample was first coated in 50 nm of alumina to provide a thermal insulation during laser heating and to help prevent diamond embrittlement from hydrogen diffusion. For electrical measurements, five bilayer tungsten-gold electrodes were sputtered/evaporated directly onto one of the diamond anvils.

A lanthanum film of thickness 260 nm was deposited onto the electrodes in a vacuum $\sim 10^{-7}$ mbar after multiple premelts to remove oxide impurities from the La source. The La film was capped with a 5 nm layer of palladium to act as an oxidation barrier and to catalyze hydrogen diffusion into the La sample [15].

Due to the hygroscopic nature of AB, we first purified by sublimation to remove any residual moisture and impurities. Loading of the AB into the gasket indentation and

initial cell closing were done in an inert Ar atmosphere in a glove box with residual O_2/H_2O < 0.5 ppm. The sample was pressurized to 95 GPa with NH_3BH_3 serving as the pressure transmitting medium (PTM).

The pressure was determined from the Raman shift of the diamond edge using the Akahama scale [24] (see Fig. S7 of the Supplemental Material [16]). The unit-cell volumes extracted from Le Bail refinement of residual lanthanum (*Fmmm*) and gold ($Fm\bar{3}m$) from the electrodes are consistent with the pressure measured using the diamond edge [25,26] (see Fig. S8 of the Supplemental Material [16]).

The La film was characterized with resistance measurements prior to laser heating (Fig. S9 of the Supplemental Material [16]), confirming metallic behavior with residual resistance ratio (RRR) ~ 2.5. The superconducting transition of pure La is observed with $T_c = 8.6$ K at 95 GPa, which is $\sim$1 K higher than reported in previous studies [25], and may originate from a pressure gradient across the sample (see sample photographs in Fig. S10 of the Supplemental Material [16]).

Synthesis of La_4H_{23} was achieved through heating of the sample and hydrogen donor material AB using a 100 W ytterbium-doped fiber laser ($\lambda = 1070$ nm) [27], with multiple 300 ms pulses. Laser power was incremented after each successive pulse until glowing was observed, indicating a temperature of $\sim$1000 K. The four-point resistance was monitored during heating, where the normal state resistance increased by a factor of $\sim$20, indicating a chemical reaction between the La film and hydrogen released from the AB. No further heating of the sample was carried out after the first observed glowing and resistance increase. As a result, some residual elemental lanthanum remained as evidenced in XRD.

X-ray diffraction was carried out at the I15 extreme conditions beam line at Diamond Light Source with Pilatus3 X CdTe 2M area detector, wavelength $\lambda = 0.425$ Å (sample-to-detector distance 385 mm). The beam was collimated to 20 μm. The calibrant used was LaB_6. Integration of the powder pattern and removal of spurious reflections were done in DIOPTAS [28]. Background subtraction of the integrated pattern and structural refinements were done in GSAS II [29].

Visualization of sample reflections on the azimuthal (cake) plot in Fig. 1(b) was enhanced by performing a background subtraction. A background image was generated using the "Minimum Frames" function in the DAWN software [30] from a spatial mapping performed over a 55×55 μm^2 region over the culet area. This background image was then subtracted from the detector image in DIOPTAS and contrast adjusted to enhance sample reflections. The integrated intensity presented in Fig. 1(a) was subject only to a standard polynomial background subtraction of the raw integrated pattern in GSAS II without any image background subtraction.

Electrical transport measurements were done in a four-point configuration with an excitation current of 10 μA using either an SRS SIM921 AC resistance bridge or an SR830 lock-in amplifier. Magnetic field studies were done at the University of Bristol with a Cryogenic Ltd magnet capable of fields up to 14 T.

Data are available at the University of Bristol data repository [31].

Acknowledgments. The authors are grateful for discussions with Lewis Conway and Tim Strobel. This work was carried out with the support of Diamond Light Source, instrument I15 (Proposal No. CY35426-1). This work was supported by ERC Horizon 2020 programme under Grant No. 715262-HPSuper and the EPSRC under Grant No. EP/V048759/1. O.L. acknowledges support from the Royal Society in the form of a University Research Fellowship (Grant No. UF150057) and associated grants.

[1] M. Somayazulu, M. Ahart, A. K. Mishra, Z. M. Geballe, M. Baldini, Y. Meng, V. V. Struzhkin, and R. J. Hemley, Evidence for superconductivity above 260 K in lanthanum superhydride at megabar pressures, Phys. Rev. Lett. **122**, 027001 (2019).

[2] A. P. Drozdov, P. P. Kong, V. S. Minkov, S. P. Besedin, M. A. Kuzovnikov, S. Mozaffari, L. Balicas, F. F. Balakirev, D. E. Graf, V. B. Prakapenka, E. Greenberg, D. A. Knyazev, M. Tkacz, and M. I. Eremets, Superconductivity at 250 K in lanthanum hydride under high pressures, Nature (London) **569**, 528 (2019).

[3] P. Kong, V. S. Minkov, M. A. Kuzovnikov, A. P. Drozdov, S. P. Besedin, S. Mozaffari, L. Balicas, F. F. Balakirev, V. B. Prakapenka, S. Chariton, D. A. Knyazev, E. Greenberg, and M. I. Eremets, Superconductivity up to 243 K in the yttrium-hydrogen system under high pressure, Nat. Commun. **12**, 5075 (2021).

[4] C. J. Pickard, I. Errea, and M. I. Eremets, Superconducting hydrides under pressure, Annu. Rev. Condens. Matter Phys. **11**, 57 (2020).

[5] W. Chen, X. Huang, D. V. Semenok, S. Chen, D. Zhou, K. Zhang, A. R. Oganov, and T. Cui, Enhancement of superconducting properties in the La-Ce-H system at moderate pressures, Nat. Commun. **14**, 2660 (2023).

[6] D. Laniel, F. Trybel, B. Winkler, F. Knoop, T. Fedotenko, S. Khandarkhaeva, A. Aslandukova, T. Meier, S. Chariton, K. Glazyrin, V. Milman, V. Prakapenka, I. A. Abrikosov, L. Dubrovinsky, and N. Dubrovinskaia, High-pressure synthesis of seven lanthanum hydrides with a significant variability of hydrogen content, Nat. Commun. **13**, 6987 (2022).

[7] M. Peña-Alvarez, J. Binns, M. Martinez-Canales, B. Monserrat, G. J. Ackland, P. Dalladay-Simpson, R. T. Howie, C. J. Pickard, and E. Gregoryanz, Synthesis of Weaire-Phelan barium polyhydride, J. Phys. Chem. Lett. **12**, 4910 (2021).

[8] K. Tanaka, J. Tse, and H. Liu, Electron-phonon coupling mechanisms for hydrogen-rich metals at high pressure, Phys. Rev. B **96**, 100502(R) (2017).

[9] J. A. Flores-Livas, L. Boeri, A. Sanna, G. Profeta, R. Arita, and M. Eremets, A perspective on conventional high-temperature superconductors at high pressure: Methods and materials, Phys. Rep. **856**, 1 (2020).

[10] D. An, D. Duan, Z. Zhang, Q. Jiang, H. Song, and T. Cui, Thermodynamically stable room-temperature superconductors in Li-Na hydrides under high pressures, arXiv:2303.09805.

[11] Z. Li, X. He, C. Zhang, K. Lu, B. Min, J. Zhang, S. Zhang, J. Zhao, L. Shi, Y. Peng, S. Feng, Z. Deng, J. Song, Q. Liu, X. Wang, R. Yu, L. Wang, Y. Li, J. D. Bass, V. Prakapenka *et al.*, Superconductivity above 70 K observed in lutetium polyhydrides, Sci. China Phys. Mech. Astron. **66**, 267411 (2023).

[12] D. V. Semenok, D. Zhou, A. G. Kvashnin, X. Huang, M. Galasso, I. A. Kruglov, A. G. Ivanova, A. G. Gavriliuk, W. Chen, N. V. Tkachenko, A. I. Boldyrev, I. Troyan, A. R. Oganov, and T. Cui, Novel strongly correlated europium superhydrides, J. Phys. Chem. Lett. **12**, 32 (2020).

[13] E. Siska, G. A. Smith, S. Villa-Cortes, L. J. Conway, R. J. Husband, J. Van Cleave, S. Petitgirard, V. Cerantola, K. Appel, C. Baehtz *et al.*, Ultra-fast yttrium hydride chemistry at high pressures via nonequilibrium states induced by x-ray free electron laser, arXiv:2307.11293.

[14] J. Guo, G. Shutov, S. Chen, Y. Wang, D. Zhou, T. Cui, X. Huang, and D. Semenok, Stabilization of high-temperature superconducting A15 phase La_4H_{23} below 100 GPa, arXiv:2307.13067.

[15] E. Snider, N. Dasenbrock-Gammon, R. McBride, X. Wang, N. Meyers, K. V. Lawler, E. Zurek, A. Salamat, and R. P. Dias, Synthesis of yttrium superhydride superconductor with a transition temperature up to 262 K by catalytic hydrogenation at high pressures, Phys. Rev. Lett. **126**, 117003 (2021).

[16] See Supplemental Material at http://link.aps.org/supplemental/10.1103/PhysRevB.109.L020503 for further details of calculated x-ray peak positions for other reported lanthanum hydride phases, pressure measurement using the Akahama scale, structural and electrical characterisation of elemental lanthanum and sample photographs.

[17] F. Belli and I. Errea, Impact of ionic quantum fluctuations on the thermodynamic stability and superconductivity of $LaBH_8$, Phys. Rev. B **106**, 134509 (2022).

[18] K. Momma and F. Izumi, Vesta: A three-dimensional visualization system for electronic and structural analysis, J. Appl. Crystallogr. **41**, 653 (2008).

[19] A. P. Drozdov, M. I. Eremets, I. A. Troyan, V. Ksenofontov, and S. I. Shylin, Conventional superconductivity at 203 kelvin at high pressures in the sulfur hydride system, Nature (London) **525**, 73 (2015).

[20] I. Errea, F. Belli, L. Monacelli, A. Sanna, T. Koretsune, T. Tadano, R. Bianco, M. Calandra, R. Arita, F. Mauri *et al.*, Quantum crystal structure in the 250-kelvin superconducting lanthanum hydride, Nature (London) **578**, 66 (2020).

[21] I. Errea, M. Calandra, C. J. Pickard, J. R. Nelson, R. J. Needs, Y. Li, H. Liu, Y. Zhang, Y. Ma, and F. Mauri, Quantum hydrogen-bond symmetrization in the superconducting hydrogen sulfide system, Nature (London) **532**, 81 (2016).

[22] T. Baumgartner, M. Eisterer, H. W. Weber, R. Flükiger, C. Scheuerlein, and L. Bottura, Effects of neutron irradiation on pinning force scaling in state-of-the-art Nb_3 Sn wires, Supercond. Sci. Technol. **27**, 015005 (2014).

[23] I. Osmond, O. Moulding, S. Cross, T. Muramatsu, A. Brooks, O. Lord, T. Fedotenko, J. Buhot, and S. Friedemann, Clean-limit superconductivity in $Im\bar{3}m$ H_3S synthesized from sulfur and hydrogen donor ammonia borane, Phys. Rev. B **105**, L220502 (2022).

[24] Y. Akahama and H. Kawamura, Pressure calibration of diamond anvil Raman gauge to 310 GPa, J. Appl. Phys. **100**, 043516 (2006).

[25] W. Chen, D. V. Semenok, I. A. Troyan, A. G. Ivanova, X. Huang, A. R. Oganov, and T. Cui, Superconductivity and equation of state of lanthanum at megabar pressures, Phys. Rev. B **102**, 134510 (2020).

[26] K. Takemura and A. Dewaele, Isothermal equation of state for gold with a He-pressure medium, Phys. Rev. B **78**, 104119 (2008).

[27] O. T. Lord, E. T. Wann, S. A. Hunt, A. M. Walker, J. Santangeli, M. J. Walter, D. P. Dobson, I. G. Wood, L. Vočadlo, G. Morard, and M. Mezouar, The NiSi melting curve to 70 GPa, Phys. Earth Planet. Inter. **233**, 13 (2014).

[28] C. Prescher and V. B. Prakapenka, DIOPTAS: A program for reduction of two-dimensional x-ray diffraction data and data exploration, High Press. Res. **35**, 223 (2015).

[29] B. H. Toby and R. B. Von Dreele, GSAS-II: The genesis of a modern open-source all purpose crystallography software package, J. Appl. Crystallogr. **46**, 544 (2013).

[30] M. Basham, J. Filik, M. T. Wharmby, P. C. Chang, B. El Kassaby, M. Gerring, J. Aishima, K. Levik, B. C. Pulford, I. Sikharulidze *et al.*, Data analysis workbench (DAWN), J. Synchrotron Radiat. **22**, 853 (2015).

[31] S. Friedemann, Dataset for publication "High-temperature superconductivity in La_4H_{23} below 100 GPa" (2023), https://doi.org/10.5523/bris.22buhfhub62xs2c7xv5w0pa10d.